CELLULAR UPTAKE OF L-LACTATE IN MOUSE DIAPHRAGM

ALAN KOCH, BRUCE WEBSTER, AND SHERMAN LOWELL, *Departments of Zoology and Mathematics, and Computer Sciences, Washington State University, Pullman, Washington, 99164*

ABSTRACT Early uptake curves of L-lactate and of mannitol were measured in quartered, incubated mouse diaphragms. Uptake was determined at 15, 30, and 45 s for various concentrations of lactate in the external solution as well as in the presence and absence of the competitive inhibitor of lactate transport, α-cyano-4-hydroxycinnimate. In normal preparations, when the external lactate concentration was 10 mM or less, the ratio of lactate-to mannitol space in the tissue was 1.7. This value was nearly independent of time and of external concentration. In normal preparations, when the external lactate concentration was >10 mM, the ratio of lactate-to-mannitol space rose with time. At a fixed time, however, this ratio fell with increasing lactate concentration. In the inhibited preparations, the ratio of lactate-to-mannitol space rose with time at all concentrations. When lactate concentration was >5 mM, this ratio was independent of the external concentration. The results suggest that there are two modes of lactate entry into these muscle cells. Entry can occur by means of a saturable system. When external lactate concentration is low, entry rates for this process are rapid compared with diffusional rates. This system probably saturates at concentrations near 10 mM and can facilitate transport in either direction. In addition, an appreciable passive leak is present. This leak accounts for about one fourth of the membrane transfer when external lactate is low, but is equal to the carrier transfer when lactate concentration is 30 mM. A model was developed to describe the entry of a permeating solute, such as lactate, into an isolated tissue.

INTRODUCTION

Lactate crosses the membranes of skeletal muscle cells quite rapidly. Fast glycolytic muscles may produce lactate at high rates during strenuous activity and must therefore eliminate it rapidly. Slow oxidative muscle, such as diaphragm, normally uses lactate as a substrate. Roos (1975) and Mainwood and Worsley-Brown (1975) have shown that lactate movement across rat diaphragm sarcolemma is passive and that it proceeds via nonionic diffusion. However, these experiments do not define whether the movement of the un-ionized form is by free diffusion or is carrier mediated.

Eggleton et al. (1928), Karpatkin et al. (1964), Karlsson (1971), Hirche et al. (1972, 1975), and Jorfeldt et al. (1978) have concluded that transmembrane movement in skeletal muscle saturates with increasing lactate concentration. Glaviano (1965) and Kubler et al. (1966) also claim to have shown saturation kinetics in cardiac muscle. Finally, a transport system has been shown in two isolated cell systems. Halstrap (1976) has shown that there are two transport systems in erythrocytes, one of which clearly saturates. Spencer and Lehninger (1976) have shown a saturable system in mouse ascites tumor cells. These two transport systems have also been shown to be inhibited by the structural analogue, α-cyano-4-hydroxy-cinnimic acid (CHC).

The issue is not as clear as it can be made to seem, however. Some of the experiments on skeletal muscle have been performed on isolated tissues. Since the transmembrane movement of lactate is probably quite rapid, its time-course might well be fast with respect to that for diffusion into the total tissue. In this case, the diffusion process, rather than the transmembrane movement, is measured. Most of the experiments on skeletal muscle have been performed with intact, perfused preparations. Here, if the time-course for transmembrane movement is rapid compared with that for transendothelial passage, distorted results can be obtained. If there is progressive vasodilatation during the time that cellular lactate is rising, a completely passive system would generate results that looked like saturation. It seems that, although there is clearly a saturating system in two types of isolated cells, there are enough difficulties in the interpretation of experiments on whole muscle to render the present evidence inconclusive.

We devised a method of transient analysis designed to circumvent the difficulties listed above. We used this method to investigate the nature of lactate transfer across mouse diaphragm cells. In addition, we used the inhibitor CHC to test whether cellular lactate uptake could be competitively modified. The results corroborate the previous conclusions that there is a carrier-mediated process for lactate movement. They also suggest that there is an appreciable leak for free diffusion.

METHODS

Swiss Webster mice weighing between 20 and 30 g were used. The mice were anesthetized with sodium pentobarbital and the whole diaphragm, with ribs attached, was removed within 45 s of the onset of surgery in a manner similar to that used by Creese (1954). The excess tissue on the ribs was not dissected away at this time. After removal, the diaphragms were placed in a bath of synthetic interstitial fluid (SIF) that used gluconate and sucrose as osmotic replacements for organic anions. The solution was modified from that of Bretag (1969); its composition is given in Table I. The batch was aerated by vigorous bubbling with 5% CO_2–95% O_2 and maintained at 40°C. Whole diaphragms were used when the thickness of the diaphragm was estimated and in experiments measuring production and utilization of lactate. The diaphragms were quartered for the experiments in which lactate uptake, mannitol uptake or surface-to-weight relations were measured. Each diaphragm was cut into four sections and the crural region was removed. The cuts were made parallel to the superficial fibers, which can be seen to run radially. The four sections, with pieces of rib still attached, were reinserted into the first bath and incubated for 5–10 min. The tissues were rinsed in a second bath of SIF for 30 s before they were used.

Physical Characteristics

Thickness of incubated diaphragms was estimated using a micrometer accurate to 0.01 mm. Each diaphragm was measured several different times and places. To test the constancy of the ratio of surface area to weight, 24 pieces of diaphragm from six mice were weighed to 0.1 mg. The pieces were then placed on a glass plate along with a calibrating spot of known area. The plate was placed in a photo enlarger and the areas of the diaphragm pieces were determined by planimetry.

Lactate Production and Use

Lactate production was determined by anaerobic incubation of whole diaphragms in 5 ml of SIF. The diaphragms weighed between 80 and 120 mg. The solution was covered with paraffin oil and bubbled with nitrogen gas. After a 20-min preincubation, 20-μl samples of bath were taken every 5 min for 0.5 h. The samples were frozen and later assayed for lactate. Lactate utilization rates were estimated by incubating mouse diaphragms in 5 ml of SIF, which contained 8.9 mM lactate and was well oxygenated.

TABLE I
COMPOSITION OF SYNTHETIC INTERSTITIAL FLUID

Cation	Concentration	Anion	Concentration	Neutral	Concentration
	mmol/liter		*mmol/liter*		*mmole/liter*
Na^+	145.2	$Cl-$	115.3	dextrose	5.55
K^+	4.50	HCO_{3-}	26.2	sucrose	7.60
$Ca^{2}+$	1.53	H_2PO_{4-}	1.67		
$Mg^{2}+$	0.69	SO_4^{2-}	0.69		
		gluconate	9.64		

When sodium lactate or sodium CHC was present, it replaced sodium chloride.

After an initial preincubation period, 20-μl samples were taken every 15 min for 2 h. The samples were then assayed for lactate.

Uptake Experiments

LACTATE UPTAKE After rinsing in the second bath, the pieces of tissue were placed in a third bath. This bath contained 20 ml of SIF with one of seven concentrations of L-lactate. The lactate was added as the sodium salt and replaced sodium chloride in SIF. Levorotatory ^{14}C-lactate and ^{3}H-mannitol were also present, each at a concentration of ~1 μC/ml. Diaphragms from six mice were used at each lactate concentration. One of the four sections of diaphragm was incubated for each of the time periods, 15, 30, and 45 s. Paired 5-μl samples of bathing solution were taken at several periods during the experiment. One sample was frozen and later assayed for stable lactate. The second sample was placed in a liquid scintillation vial along with the fourth piece of diaphragm.

The uptake of lactate was also determined in the presence of the inhibitor CHC. For these experiments, both the second and the third bath contained 20 mM CHC.

MANNITOL UPTAKE Mannitol was used as the extracellular marker. The uptake of mannitol was measured following a similar experimental protocol. Data from seven periods, ranging from 2–30 min, were collected after a lactate-free incubation.

Analytical Techniques

Estimation of stable lactate was made using the flurometric assay of Lowry (1972). Although it is not important in the present experiments, CHC interfered with chemical determination of lactate. The inhibitor absorbs light in a broad band extending from 300–460 nm. This range includes both the excitation wavelength of 340 nm and the emission wavelength of 450 nm. Calibration curves using the various diluted concentrations of CHC found in the lactic acid dehydrogenase-NADH reaction mixture were linear. However, the readings were very low and the accuracy of lactate determination was poor in the presence of CHC.

All isotope counting was done by liquid scintillation. At the end of the incubation periods, the diaphragm was removed and quickly dipped in SIF at room temperature. The excess solution was gently wiped from the sample and the diaphragm was cut away from the ribs and blotted. The time from end of incubation until blotting was <5 s. The muscle piece was weighed to 0.1 mg; weights varied between 5 and 20 mg. After weighing, the tissue was put into a liquid scintillation vial containing 0.5 ml Baker tissue solubilizer. The tissue was digested, neutralized with glacial acetic acid, and 12 ml of either Aquasol (New England Nuclear Corp., Boston, Mass.) or Scintiverse (Fisher Scientific, Pittsburgh, Pa.) were added. The vials were counted to 20,000 counts. Samples were checked for chemiluminesence; repeat counts were normally within counting error. Recovery of added isotope showed that quenching was always negligible with the amounts of tissue used in these experiments. Count rates were separated using standard dual channel isotope procedures. Lactate and mannitol spaces were determined as activity ratios, i.e., cpm/gm tissue divided by cpm/cm^3 bathing fluid.

RESULTS

Physical Characteristics

Muscle thickness was calculated from triplicate measurements of three whole mouse diaphragms. The mean thickness was 0.266 ± 0.08 mm (SEM). The ratio of weight to surface area was found to be relatively constant. 24 pieces of diaphragm from six mice were measured. The mean ratio was 37.64 ± 0.99 mg/cm^2 (SEM). The low coefficient of variation indicates that the surface area available to diffusional entry can be taken as proportional to the weight of the sample.

Lactate Production and Use

The net rate of lactate use was taken as the slope of the line determined from the linear regression of the decrease in total bath concentration with time. The bath had four diaphragms in it. The slope divided by the total weight was computed as the rate of utilization per unit weight. Well-oxgenated diaphragm used lactate at a rate of 0.0915 μ mol/min · g wet weight. Production was measured individually on each of three diaphragms. The regression slopes were divided by the respective weights and the mean production rate was calculated. Under anaerobic conditions, diaphragm released lactate at a mean rate of 2.59 ± 0.23 μ mol/min · g wet weight (SEM).

Mannitol Uptake

The uptake kinetics of the extracellular marker mannitol were determined. These kinetics defined the volumes of the fluid compartments as well as the tortuosity factor (ϵ). The tortuosity factor is the ratio of the real distance a particle must travel as it passes around the muscle cells to the measured linear distance. (Brookes and MacKay, 1971). This factor is greater than would be expected from geometric considerations. This experiment pointed up one of the hazards in the approach used here. Occasionally, an appreciable number of fibers are cut in the quartering procedure. When this occurs, the mannitol space is abnormally high. Thus, in these experiments, the average mannitol space was 0.135 ml/g tissue at 3 min. However, one sample showed a mannitol space >0.29 ml/g tissue. This value was discarded. Two samples were discarded from the 30-min time because of excessively large mannitol spaces. No samples were discarded that showed mannitol spaces within 3 SEM of the remaining samples and no samples were discarded because of very low values. The mannitol spaces obtained from these seven time periods, along with those obtained from the three times in the lactate experiments, were used to fit the equation of diffusion into a plane sheet. The solution of this problem is given in Eq. 1 where V_e is the extracellular volume in milliliters per gram of wet tissue.

$$\text{space} = V_e\left(1 - \frac{8}{\pi^2}\sum_{n=0}^{\infty}\frac{\exp\left[-(2n+1)^2\theta t\right]}{[2n+1]^2}\right). \quad (1)$$

The parameter θ is equal to $\pi^2 D/4l^2\epsilon^2$ where D is the diffusion coefficient in cm^2/s and the thickness of the diaphragm is $2l$. The data were fit to the first four terms of the series by means of a nonlinear least-squares fitting routine. Extracellular fluid volume was estimated to be 0.277 ml/g and θ was estimated as 0.00292 s^{-1}. The mannitol spaces and the computed curve are illustrated in Fig. 1. Using the value of 0.0133 cm for l that was obtained above and

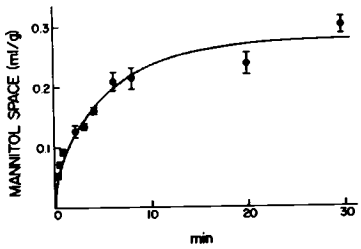

FIGURE 1

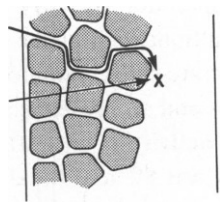

FIGURE 2

FIGURE 1 Uptake of mannitol by mouse diaphragm. The mannitol space (ml/g) is plotted as a function of time (min). The first three values are taken from the lactate uptake experiments and are the average of 68, 70, and 67 determinations, respectively. The values from 2 min on are usually averages of six determinations. The brackets include 1 SEM. The solid line is a plot of Eq. 1 using the values $V_e = 0.277$ ml/g and $\theta = 0.00292\ s^{-1}$.

FIGURE 2 Paths for entry. Upper line, long extracellular path; lower line, direct transcellular path. X is a typical extracellular region within the tissue.

the value of 6.85×10^{-6} cm^2/s for the diffusion coefficient of mannitol (Handbook of Chemistry and Physics, 1968), we computed a value of 5.7 for ϵ. It is also possible to compute ϵ from the mannitol uptake in the lactate uptake experiments. These experiments involve only the earliest portions of the uptake curve, but there are a very large number of experimental points available. 67–70 points are available for each of the three times at which samples were collected. An approximate solution for this early uptake is given in Eq. 2. The points for these early mannitol spaces fell on a good straight line that passed through the origin when plotted as a function of the square root of time.

$$\text{space} = \frac{V_e}{\epsilon}\left(\frac{4D}{\pi l^2}\right)^{0.5} t^{0.5} \tag{2}$$

The slope of this plot was 0.0142 ml $\cdot$ g^{-1} s$^{-0.5}$. This value leads to a calculated value of 4.3 for ϵ. Thus, the tortuosity in fresh mouse diaphragm is ~5.

Lactate Uptake

Lactate uptake was determined at seven different concentrations in normal diaphragms and at five different concentrations in the presence of 20 mM CHC. For each concentration, the lactate and mannitol contents of the tissue were determined at 15, 30, and 45 s. During this time period, both the entry of lactate from the bath into the interstitial fluid and the entry of lactate from interstitial fluid into cells were occurring rapidly. Characterization of the cellular uptake process depends on knowing the time-course of lactate entry into interstitial fluid. The simultaneously determined mannitol spaces gave an indication of interstitial entry. The results will therefore be presented in terms of ratios of the lactate space to the mannitol space (R) for either the normal or the inhibited preparation. Since oxygenated diaphragms produced negligible lactate (see above), isotope activities rather than specific activities were used to compute tissue spaces.

The diffusion coefficient of mannitol is different from that of lactate. Eggleton et al. (1928) measured the diffusion coefficient of lactate in agar and obtained a result of 1.1×10^{-5} cm^2/s. We estimated the diffusion coefficient of lactate in water on the basis of its molecular

dimensions and arrived at a figure of 1.05×10^{-5} cm^2/s. This value is 1.54 times the diffusion coefficient of mannitol. At early times, diffusion proceeds as the square root of the diffusion coefficient. Multiplication of the mannitol spaces by 1.24 (the square root of 1.54) gives the space that a lactate-sized mannitol would have had. Ratios of R divided by 1.24 will be termed corrected ratios and all subsequent data will be presented as corrected ratios.

The isotope activity in the bath fell during each experiment. The maximum decrease in lactate activity was 8% and the decrease in mannitol activity was smaller. We computed the linear regressions of both lactate and mannitol isotope activity and calculated the spaces as the ratio of the tissue content per gram divided by the interpolated bathing solution activity. Stable lactate concentration also fell with time in the external bath in all experiments except those with the lowest external lactate concentration. It fell at most 4% and was simply taken as the time-average concentration.

The mannitol spaces determined during the lactate experiments were not affected either by changes in lactate concentration or by the presence of the inhibitor. As in the mannitol experiments, there were occasional preparations that showed inordinately high mannitol spaces. The same criteria were used for rejection as were used in the mannitol experiments.

LACTATE SPACES AS A FUNCTION OF EXTERNAL LACTATE TABLE II presents the values of corrected R at 30 s for each concentration in both the normal and inhibited preparations. In the normal preparation, when external lactate was <12 mM, there was no clear dependence of the space ratio on concentration. The average of R was ~1.7 at these lower concentrations. As the concentration of lactate rose, R fell until it was <1.2 when external lactate was 27.5 mM. The inhibited preparation gave rise to much lower values of R and showed no consistent concentration dependence. The value of R for these preparations was ~1.2 at 30 s. Earlier and later spaces showed similar behavior.

TABLE II
RATIOS OF THE LACTATE TO THE MANNITOL SPACE AT 30 s

Concentration*	R‡	+ Slope/total§	P‖
mM			
Normal			
1.55	1.62 (0.08)	2/5	0.4
5.12	1.64 (0.08)	1/6	0.17
6.48	1.76 (0.15)	2/6	0.33
11.48	1.64 (0.09)	4/6	0.67
13.93	1.43 (0.09)	3/5	0.60
21.7	1.50 (0.05)	3/6	0.50
27.5	1.16 (0.03)	4/5	0.80
Inhibited			
2.83	1.55 (0.10)	3/6	0.50
5.50	1.19 (0.04)	4/6	0.67
11.50	1.14 (0.04)	5/5	1.00
14.00	1.19 (0.05)	5/6	0.83
25.19	1.21 (0.06)	5/6	0.83

*Concentration of stable lactate in the incubation medium.
‡Corrected 30-s space ratio SEM.
§Number of animals that showed a positive slope divided by the total number of animals.
‖*a-posteriori* probability that the slope is positive.

In addition to determining R at a fixed time as a function of external concentration, it was of interest to evaluate the way R changed in time for each concentration. An estimate to the time derivative was obtained from the difference between the 45 and 15 s value of R for each mouse. This derivative ($\dot{R}$) was regarded as positive if the 45-s value was at least 0.01 > 15-s value. The last column of Table II shows the fraction of animals at each concentration for which a positive slope in time was obtained. In 29 experiments with the inhibitor, 22 showed a positive slope. A binomial test indicates that the probability of observing this result from a universe that did not really have a positive slope is <0.005. The normal preparations showed a different pattern. Only at the highest concentration of lactate was a positive value of $\dot{R}$ a common result. At low concentrations of lactate the most common result was a small negative value of $\dot{R}$. Indeed, for the 17 animals examined when lactate concentration was <10 mM, there was only a 7% likelihood that the results came from a universe characterized by positive $\dot{R}$. The data suggest that, in the normal preparation, $\dot{R}$ is zero or negative when the external lactate is low, but positive at higher external concentrations.

The probability of observing a positive $\dot{R}$ is strongly correlated to the 30-s value of R. The overall correlation coefficient between these variables was −0.85. If these variables are plotted against each other, the data are described by a straight line with a negative slope near 1. The apparently anomalous value of R observed at 2.8 mM lactate in the inhibited preparation shows a correspondingly low probability and fits into this correlation.

DISCUSSION

Methodology and Accuracy

To determine the cellular uptake of lactate accurately, the isotope that enters the cells must remain there. However, lactate is metabolized and this metabolism leads to the loss of some of the label as radioactive CO_2. We can determine the importance of this distortion by comparing the utilization rates of lactate to its total entry rates into muscle tissue. We obtained a rate of utilization of 91.5 n mol/min · g; this rate was obtained when external lactate was 8.9 mM and the incubation temperature was 40°C. Bendall and Taylor (1970) determined the lactate utilization rate as a function of external lactate concentration in frog sartorius muscle. In that preparation, utilization was nearly proportional to concentration over the range of interest here. They also determined lactate metabolism in rabbit psoas muscle when the external concentration was 45 mM and the incubation temperature was 24°C. Their value was 66 nmol/min · g. Our data suggests the presence of two parallel pathways (see below). Using the concentration dependencies we found, we would estimate that the influx would be about twice as rapid when external lactate is 45 mM as when it is 9 mM. If the Q_{10} of the total transport is near 2, lactate would become available to cellular utilization in our experiments at about one and one-half times the rate at which it was available in the experiments of Bendall and Taylor (1970). Thus, our utilization rates for mouse diaphragm are similar to theirs for rabbit psoas. We can also estimate the rate of entry of lactate into the tissue and compare the two rates. Table III presents the results of this comparison for the highest and lowest concentrations of lactate. At intermediate concentrations, utilization and uptake rates and ratios all had intermediate values. Lactate utilization was never as high as 2% of the rate at which it entered the tissues. We conclude that lactate utilization never

TABLE III
COMPARISON OF UTILIZATION RATE WITH TISSUE UPTAKE

Concentration	Average utilization	Average uptake	Ratio
mmol/liter	*nmol/g tissue · min*	*nmol/g tissue · min*	
1.55	3	397	0.008
27.5	58	4371	0.013
5.5*	12	1058	0.011
25.19*	53	3661	0.015

The values were computed as averages over the 45-s duration of the experiments. The tissue uptake rate was computed as the lactate space at 45 s times the external concentration divided by 0.75. Average utilization was computed as the average fraction of the amount of the tissue involved times the external concentration divided by 8.9.

*Inhibited preparations.

distorted our results in a measurable way. It should be pointed out that the fluxes shown in Table III are for the total entry of lactate into the tissue and do not describe transmembrane movement.

In the Methods section, we commented on the difficulty of measuring stable lactate in the presence of CHC. These problems did not affect the accuracy of our determinations of R since that ratio was determined isotopically. The only uncertainty is the concentration of stable lactate at which the experiments were conducted and this uncertainty is <10%. Inasmuch as there was no concentration dependence of R in the inhibited preparations, we do not regard this analytic difficulty as affecting our interpretations.

We estimated the extracellular space as 0.277 ml/g. Evans and Smith (1976) found a value of 0.28 ml/g for mouse diaphragm. The tortuosity factor that we estimated is higher than those that have been estimated for rat diaphragm. Creese (1954) found a value of ~2. Brookes and MacKay (1971) investigated the time-dependence of ϵ. Their earliest values were obtained at ~40 min and averaged 4.4. Extracellular space increased with time and ϵ fell until it finally approached the low values of Creese. The value of ϵ we found was ~5. The combination of a high value for ϵ with agreement in the estimates of extracellular space leads us to believe that our preparations were in good physiologic condition.

Experimental estimation of derivatives is inherently a noisy process and when this process is applied to data that are quite variable, the numerical results do not have much meaning. We do not have much confidence in the numerical values we obtained for $\dot{R}$ and feel that tenable conclusions must be based on the sign of this variable.

Analysis of the Transport

The basic interpretation of the results presented in Table II seems clear. If the cellular entry of lactate were free diffusion, R would have been independent of the external concentration. Further, the inhibitor CHC would not be expected to change R. The data contradict both of these expectations and we therefore conclude that lactate enters muscle cells via a saturable, carrier-mediated transport system. Our findings therefore corroborate the conclusions listed above.

There are some peculiar features to the data. Most striking was, at low concentrations of lactate, $\dot{R}$ was near zero or negative in the normal preparation. A second peculiarity is more

subtle; R attained high values very quickly. We shall show below that this finding is, in itself, incompatible with the simple models of diffusional entry into tissue. Finally, the variability between mice is higher than would be expected. These features prompted a re-examination of the physical processes occurring when a solute that can cross cell membranes diffuses into an isolated tissue. The model that emerged is somewhat different from the conventional one. It predicts the apparently anomalous behavior observed here.

THE PHYSICAL PROBLEM We start with an isolated tissue made up of cells and an extracellular fluid that winds between and around the cells, ultimately to communicate with an external bathing solution. We wish to analyze how the cell membranes control the entry of a permeating solute and do this by comparing the total tissue content of the permeating solute to that of an extracellular marker. The normalized tissue content (that is, milligrams of material per gram tissue divided by the bathing concentration in milligrams per milliliter) is the tissue space and it is the spaces that are compared.[1] Since information about the kinetics of membrane transport can only come from transient experiments, it is necessary to use an extracellular marker simultaneously with the permeant solute to deduce the fraction of the total tissue content within cells.

The distances traversed during diffusion through the extracellular fluid are a good deal longer than would be estimated from external measurement of the tissue because the extracellular path around cells is tortuous. In the case of the extracellular marker, ϵ can be incorporated into a modified diffusion coefficient to give a standard diffusion equation. Spaces computed from this equation are those from the solution of the standard diffusion equation in which time has been scaled by a factor ϵ^2. Analysis of this problem has been presented by Creese (1954) and by Brookes and MacKay (1971).

Fig. 2 depicts the situation for a permeant solute. Two pathways are available to a permeant solute as it diffuses from the external bath to an interior extracellular point X. The extracellular path is available, but this is a long distance. A shortcut is also present if the solute readily crosses cell membranes. Although this direct path does require crossing cell membranes, it is shorter than the extracellular path by a factor of ϵ. Since the scaling for time depends on ϵ^2, a large fraction of the material that arrives at X got there by using the transcellular pathway when cellular permeability was reasonably high. Indeed, at high cellular permeabilities, the concentration of the permeant solute at an interior extracellular point may be much higher than the concentration of extracellular marker. When this is true, interpretation of the ratio of tissue spaces is not straightforward. Difficulty in interpretating the space is not restricted to conditions of high cell permeability. When cell permeability is low, most of the solute that arrives at point X got there via the extracellular pathway. However, the cells surrounding point X act as a sink and some of the solute that got to point X leaves the extracellular fluid to enter cells. Thus, at low cellular permeabilities, the concentration of solute at an interior extracellular point may be lower than the concentration of the extracellular marker. If the space of the marker is used to estimate the quantity of

[1]Although the text is written in terms of a chemical determination, identical considerations apply when isotope movement is compared. In the isotope experiment, specific activity is used instead of concentration and relative specific activity is used instead of space. In this experiment, production of the stable material was negligible and the specific activity of the bathing solution did not change. Activity in counts per minute was therefore used as a measure of concentration and the ratio of tissue to bathing fluid activities was a measure of the space.

extracellular solute, there is uncertainty, not only in the magnitude of the extracellular solute, but even whether there is more or less present than indicated by the marker space. Both the amount and direction of these distortions depend on the tortuosity factor, the cell permeability, and time.

POSSIBLE MODELS There are two types of models that might be used to describe the behavior of this system. The first of these is a diffusion system wherein there is simultaneous reversible chemical reaction. The reacted species is immobile. This model would describe permeation of affinite ions through an ion exchange membrane. We shall call this a Crank model because Crank has given an excellent exposition of both the mathematics and physical behavior of this system (1964).

A Crank model does not take the transcellular pathway into account, but rather assumes that solute gets to an interior extracellular point by traversing the extracellular pathways. Once there, it may rapidly enter cells and thereby lower extracellular concentration, but entry of solute into the tissue is limited by extracellular diffusion. A Crank model can be distributed and expressed as a pair of partial differential equations or it can be compartmentalized and expressed as a set of ordinary differential equations. A ladder network of resistors and capacitors can be a physical representation of a compartmentalized Crank model. The two ways of expressing the Crank model are equivalent; the general behavior is similar and solutions of the compartmental models approach the solution of the distributed model as the number of compartments is increased.

The second type of model is one that explicitly includes the transcellular pathway. Inclusion of this pathway introduces behavior that is fundamentally different from that of a Crank model. The most practical way to express the model is in compartmentalized form and to solve it as a set of ordinary differential equations. We shall derive these equations and give their solution for the simplest case. After developing the solution, we shall look at its physical behavior and compare it with that of a Crank model.

Fig. 3 shows the electrical analogues for three different models of an isolated tissue. These models are formed by cascading repeating units, which we shall term compartments. Any number of compartments may be used. Generally, the greater the number of compartments, the closer is the model behavior to that of the real tissue and the greater is the computational difficulty. The first and last compartment have special relations, so a three-compartment model is the smallest model for which representative compartmental equations are derived.

Fig. 3 *a* shows the model appropriate for the entry of an extracellular marker into the tissue. Each compartment is made up of a resistor and a capacitor. The sum of the capacitors is the extracellular volume and the value of the resistor is chosen to match the experimentally determined kinetics of uptake or leachout. We shall express all resistances in terms of their reciprocals, the conductances (σ). The set of equations derived from the network of Fig. 3 *a* is the compartmentalized version of the diffusion equation. Fig. 3 *b* shows the network that is the analogue of the Crank model. The extracellular components are the same, but additional elements have been added to represent the cellular compartment. The sum of the cellular capacitors is the cellular volume of distribution of a permeant solute and the value of the cellular conductance is chosen to match the kinetics of cell uptake. Fig. 3 *c* shows the network we propose for diffusion of a permeant solute into a tissue. The components of the Crank model are still present, but there is an additional path. The presence of this additional

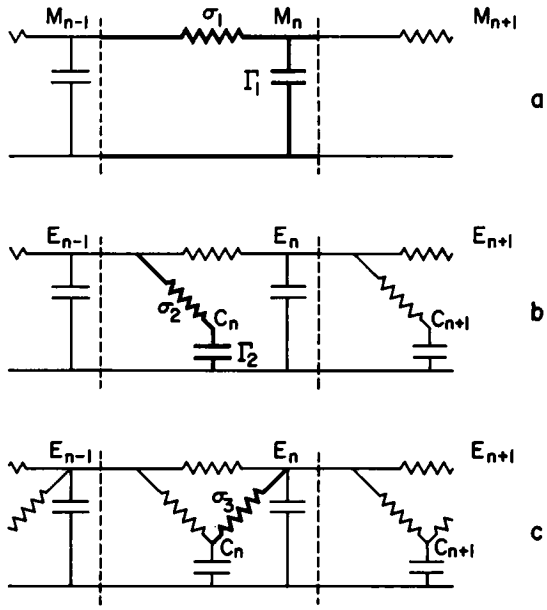

FIGURE 3 Equivalent circuits for different models: (*a*) extracellular diffusion; (*b*) the Crank model; (*c*) the proposed model. The dotted lines enclose a typical compartment.

conductance σ_3, means that it is possible for material to arrive at the interior extracellular point via a transcellular route as well as an extracellular route.

The electrical analogues look simpler if they show only three conductances. In reality, there are two conductances in series that make up σ_2. One of these is the conductance associated with diffusion through the cell itself. This is presumed to be non-tortuous diffusion of the solute and the value of this conductance (σ_c) is known from the diffusion coefficient of the permeant solute. The conductance in series with σ_c is the membrane conductance σ_λ. Since transcellular diffusion is in σ_2, σ_3 is only the membrane conductance.

The case to be solved is that of a plane sheet that has a thickness of $2l$ and is large enough to ignore edge effects. The concentration of the diffusing material is initially zero in the tissue and is always 1.0 in the bath. For a model with k compartments, application of Ohm's law across each impedance and conservation of current at each node leads to k differential equations for the extracellular fluid. When cellular uptake is present, the coupled system requires $2k$ equations. Table IV gives a list of the symobls used. A dot over a variable will be used to signify the time derivative.

Extracellular model: Let M_n be the voltage at the n^{th} node. The general relation is

$$\tau_0 \dot{M}_n = M_{n-1} - 2M_n + M_{n+1} = \delta^2 M_n \tag{3}$$

where δ^2 is the second difference operator and $\tau_0 = \Gamma_1/\sigma_1$ is the extracellular time constant. The outer compartment sees the concentration in the bathing solution, so its relation is

$$\tau_0 \dot{M}_1 = \quad - 2M_1 + M_2 + 1. \tag{4}$$

The innermost compartment goes to the center of the tissue and there is no flow beyond that

TABLE IV
SYMBOLS USED IN TEXT

Symbol	Meaning in mouse diaphragm	Equivalence in electrical analogue
C_n	concentration of lactate in nth cellular compartment (mmol or cpm/liter)	voltage for lactate at nth cellular node (V)
D	diffusion coefficient (cm^2/s)	
E_n	concentration of lactate in the extracellular space of the nth compartment (mmol or cpm/liter)	voltage for lactate at the nth extracellular node (V)
l	half thickness of the diaphragm (cm)	
M_n	concentration of mannitol in the nth compartment (mmol or cpm/liter)	voltage for mannitol at the nth extracellular node (V)
R	ratio of lactate to mannitol space	ratio of lactate charge stored on Γ_1 and Γ_2 to mannitol charge stored on Γ_1
V_e	extracellular space (ml/g tissue)	
Γ_1	extracellular volume in each compartment (ml/g tissue)	extracellular capacitance (Fd)
Γ_2	cellular volume of distribution of lactate at steady-state = cellular volume times distribution ratio (ml/g tissue)	cellular capacitance (Fd)
ϵ	tortuosity factor	
μ	eigenvalues of the equations for concentration	
σ_c	cell fluid permeability (ml/g tissue/s)	cellular conductance (S)
σ_λ	membrane permeability (ml/g tissue/s)	membrane conductance (S)
σ_1	extracellular permeability (ml/g tissue/s)	extracellular conductance, $\sigma_c/(\epsilon^2 - 1)$; (S)
σ_2	series combination of σ_c and σ_λ	$(\sigma_c\sigma_\lambda)/(\sigma_c + \sigma_\lambda)$
σ_3	membrane permeability or conductance	σ_λ
τ_0	extracellular time constant	Γ_1/σ_1
τ	cellular time constant	Γ_2/σ_2

point. Its relation is

$$\tau_0 \dot{M}_k = M_{k-1} + M_k. \tag{5}$$

Crank model: Let E_n be the voltage at the nth extracellular capacitor, Γ_1 and let C_n be the voltage at the nth cellular capacitor, Γ_2. Eq. 6 gives the general relations, Eqs. 7 and 8 give the relations for the outermost and innermost compartments.

$$\begin{aligned} \tau \dot{C}_n &= E_{n-1} - C_n \\ \tau_0 \dot{E}_n &= [\delta^2 - \sigma_1/\sigma_2]\ E_n + \sigma_2/\sigma_1 C_{n+1} \end{aligned} \tag{6}$$

$$\begin{aligned} \tau \dot{C}_1 &= -C_1 + 1 \\ \tau_0 \dot{E}_1 &= -(2 + \sigma_2/\sigma_1)E_1 + \sigma_2/\sigma_1 C_2 - E_2 + 1 \end{aligned} \tag{7}$$

$$\begin{aligned} \tau \dot{C}_k &= E_{k-1} - C_k \\ \tau_0 \dot{E}_k &= E_{k-1} - E_k \end{aligned} \tag{8}$$

where $\tau = \Gamma_2/\sigma_2$ is the cellular time constant.

Proposed model: The relations for this model are somewhat more complex. They are described by Eqs. 9–11.

$$\tau \dot{C}_n = E_{n-1} - [1 + \sigma_3/\sigma_2]C_n + \sigma_3/\sigma_2 E_n$$
$$\tau_0 \dot{E}_n = \sigma_3/\sigma_1 C_n + [\delta^2 - (\sigma_2 + \sigma_3)/\sigma_1]E_n + \sigma_2/\sigma_3 C_{n+1} \quad (9)$$

$$\tau \dot{C}_1 = -[1 + \sigma_3/\sigma_2]C_1 + \sigma_3/\sigma_2 E_1 + 1$$
$$\tau_0 \dot{E}_1 = \sigma_3/\sigma_1 C_1 - [2 + (\sigma_2 + \sigma_3/\sigma_1)]\ E_1 + \sigma_2/\sigma_1 C_2 + 1 \quad (10)$$

$$\tau \dot{C}_k = E_{k-1} - [1 + \sigma_3/\sigma_2]C_k + \sigma_3/\sigma_2 E_k$$
$$\tau_0 \dot{E}_k = E_{k-1} + \sigma_3/\sigma_1 C_k - [1 + \sigma_3/\sigma_1]E_k. \quad (11)$$

SOLUTION OF THE PROPOSED MODEL *Mathematics:* A solution can be obtained for any of the models regardless of the number of compartments used. The solutions and behavior of the diffusion model and the Crank model are well known; we shall concentrate on the solution of our model.

We write the equations for the model as

$$A\dot{\mathbf{W}} = B\mathbf{W} + \mathbf{F} \quad (12)$$

where A is the diagonal matrix of the time constants, $\mathbf{W}$ is the column vector of the variables C and E, B is the matrix of coefficients and $\mathbf{F}$ is the column vector of forcing functions. $\mathbf{F}$ is $(1, 1, 0, 0, \ldots 0)^T$. Multiplication of each equation for C by (σ_2/σ_1), renders B symmetric. Since B is also positive definite, its eigenfunctions are real and solutions for the system are always sums of exponentials. To solve the one compartment case explicitly, we use Eqs. 11 and set $E_0 = 1$. The solutions are

$$E = 1 - \frac{(1/\tau_0 - \mu_2)\, e^{-\mu_1 t} + (\mu_1 - 1/\tau_0)\, e^{-\mu_2 t}}{\mu_1 - \mu_2}$$
$$C = 1 - \frac{(1/\tau - \mu_2)\, e^{-\mu_1 t} + (\mu_1 - 1/\tau)\, e^{-\mu_2 t}}{\mu_1 - \mu_2} \quad (13)$$

where the rate constants μ_1 and μ_2 are defined by Eq. 14.

$$(Z + \mu_1)(Z + \mu_2) = Z^2 - \left[\frac{1 + \sigma_3/\sigma_1}{\tau_0} + \frac{1 + \sigma_3/\sigma_2}{\tau}\right]Z + \frac{1 + \sigma_3/\sigma_1 + \sigma_3/\sigma_2}{\tau\tau_0} = 0. \quad (14)$$

Their approximate values are

$$\mu_1 = [(1 + \sigma_3/\sigma_1)]\tau + (1 + \sigma_3/\sigma_2)]\tau_0/\tau\tau_0$$
$$\mu_2 = [1 + \sigma_3/\sigma_2 + \sigma_3/\sigma_1]/[(1 + \sigma_3/\sigma_1)\tau + (1 + \sigma_3/\sigma_2)\tau_0]$$

σ_1 is the larger root. The quantity of solute in the extracellular space is given by the charge stored on Γ_1 and the quantity of solute within cells is given by the charge stored on Γ_2. Uptake of the extracellular marker for the one-compartment case is described by Eq. 5 with M_0 taken as 1. Its solution is

$$M = 1 - \exp(-t/\tau_0) \quad (15)$$

The quantity of extracellular marker within the tissue is $\Gamma_1 M$. The ratio of permeant solute to marker space is therefore given by Eq. 16.

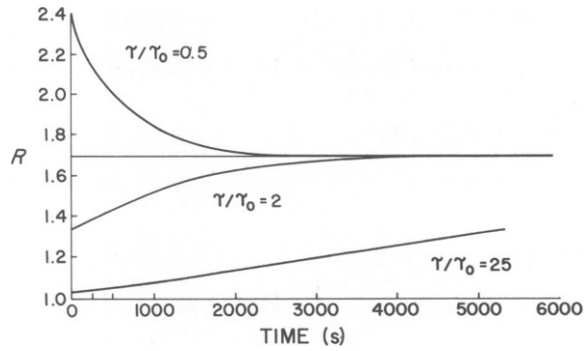

FIGURE 4 Time-course of the function ($R - 1$) for three different values of cellular permeability. Cellular permeability is expressed as the ratio of time constants, τ/τ_0. Low values of τ/τ_0 correspond to high permeability. The steady value is 0.693. Time is in seconds.

$$R = \frac{[1 + (\Gamma_2/\Gamma_1)] - \dfrac{[1/\tau_0 - \mu_2 + (\Gamma_2/\Gamma_1)(1/\tau - \mu_2)]e^{-\mu_1 t} + [\mu_1 - 1/\tau_0 + (\Gamma_2/\Gamma_1)(\mu_1 - 1/\tau)e^{-\mu_2 t}}{\mu_1 - \mu_2}}{1 - e^{-t/\tau_0}}. \quad (16)$$

Eq. 16 is the basic equation that describes the behavior of the experimentally useful measure, R. The five parameters in the solution are the two capacities and the three conductances. Γ_1 is taken as the steady-state volume of distribution of extracellular marker. Γ_2 is the cellular space of permeant solute at steady state and is determined experimentally as the difference between the steady values of the two spaces. The value of σ_1 is obtained from the kinetics of marker uptake. The other conductances are related to free diffusion (σ_c) and the conductance of the cell membrane to the permeant solute, σ_λ. When the kinetics of marker uptake and the steady-state spaces are known for both solutes, Eq. 16 is a function of time with the single undetermined parameter of permeability of the cell membrane to permeant solute. The choice of σ_λ that makes Eq. 16 match the experimental data is the estimate of the cell membrane conductance.

Physical behavior Fig. 4 shows the relation between R and time for three different values of σ_λ. The values for the other parameters were chosen to fit the mouse data. Γ_1 was 0.277 Fd, Γ_2 was 0.192 Fd, σ_1 was 4.902×10^{-4} S, and σ_c was 24 times that value or 1.1765×10^{-2} S. A convenient way to express the desired parameter, σ_λ is in terms of the variable τ/τ_0.[2] Three different values of τ/τ_0 are depicted in Fig. 4.

Several features of the behavior are immediately evident. The natural way to scale time is in terms of τ/τ_0. We have chosen not to do this because the scale is unknown until after the data is collected. At long times, R approaches its steady value of $1 + (\Gamma_2/\Gamma_1)$. In the present case, that value is 1.69. When τ/τ_0 is < 1, R starts high and falls progressively; when τ/τ_0 is $>$ 1, R starts low and rises progressively to its final value. Differences between the behaviors are largest early in the uptake. Comparison of the slopes of R indicates that, as τ/τ_0 increases, this slope increases from a negative to a positive value, passes through a maximum, and then falls

[2]As the number of compartments is increased, the match to experimental data leads to a progressive reduction of Γ_1, Γ_2, and σ_1. The value of σ_λ which fits any given set of data also decreases. However, the ratio of time constants that produces the same behavior remains similar.

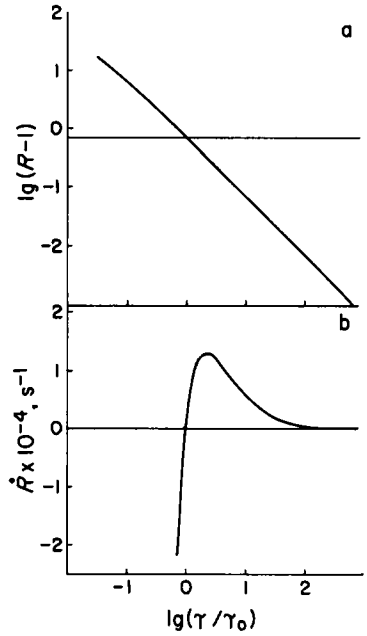

FIGURE 5

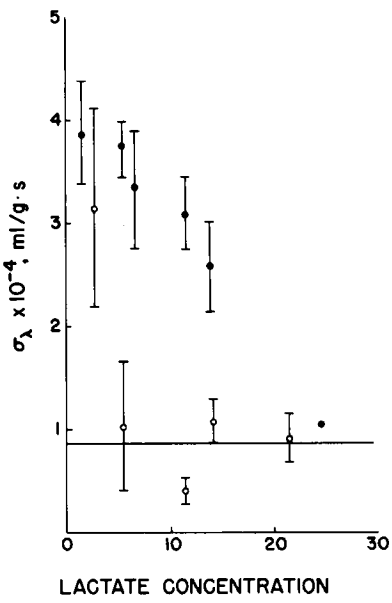

FIGURE 6

FIGURE 5 Relations between R and τ/τ_0 for one compartment models at 30 s. (*a*) Log $(R - 1)$ as a function of log (τ/τ_0). The equilibrium value of -0.16 corresponds to an equilibrium value of 1.69 for R. (*b*) $\dot{R}$ as a function of log (τ/τ_0). The relation crosses zero when $\tau = \tau_0$.

FIGURE 6 Conductances of the cell membrane to lactate (ml/g · s) as a function of external lactate concentration (mmol/liter). The experimental conductances have been multiplied by 10^4 for the figure. ●, normal preparations; ○, inhibited preparations. The brackets include 1 SEM. The horizontal line is the average of the inhibited conductances at the four higher concentrations of lactate. Its value is $0.858 \times 10^{-4} \pm 0.158$ (SEM). It is taken as an estimate of the passive flux.

toward zero. The system can be characterized by the two relations shown in Fig. 5. Fig. 5 *a* depicts the relation between R at 30 s and τ/τ_0. For the mouse data, this time is $\sim 0.05\tau_0$. For values of $\tau/\tau_0 > 0.25$, Eq. 17 is a very good approximation of τ. At lower values, $(R - 1)$ does not fall as rapidly as predicted by Eq. 17 when τ/τ_0 is increased. The relation stops when σ_λ is infinite. There, τ is Γ_2/σ_c and $\tau/\tau_0 = 0.029$. In the range of

$$\tau = \frac{\tau_0(\Gamma_2/\Gamma_1)}{R - 1} \tag{17}$$

validity of Eq. 17, the membrane permeability to the solute is given by Eq. 18.

$$\sigma_\lambda = \sigma_c \frac{R - 1}{\epsilon^2 - R} \tag{18}$$

Fig. 5 *b* shows the relation between $\dot{R}$ and τ/τ_0. At values of τ/τ_0 smaller than those shown, the slope is more strongly negative. When τ/τ_0 is low, the cellular capacitor charges more quickly than does the extracellular one. The cell is a source for the extracellular compartment and indeed, at very low values of τ/τ_0, this rapid transcellular route allows the tissue to be

filled with permeant solute at a time when extracellular marker is just beginning to enter. An early high value of R is obtained. As time passes, not much more solute enters the tissue, but the extracellular marker does enter and R falls. When τ/τ_0 is exactly equal to 1, the cellular and extracellular capacitors charge at the same rate. Since the voltages on them are always the same, there is no current through σ_3. From the perspective of E, it is as if C were not present and the behavior of E and M are identical. R immediately assumes its equilibrium value and remains there throughout uptake. When $\tau/\tau_0 > 1$, Γ_1 charges more rapidly than does Γ_2. The cellular capacitor acts as a sink for the extracellular capacitor and there is net current from E to C. The value of $\dot{R}$ shows the direction and magnitude of the current through σ_3 and because it is this current that leads to differences between E and M, $\dot{R}$ also shows how E differs from the simultaneous value of M. The fact that $\dot{R}$ passes through a maximum indicates that two different processes determine the current through σ_3. As τ/τ_0 increases, there is a monotone increase in the driving force, $E - C$. When this increase is more important than the concomitant decrease in conductance, the net inward current through σ_3 increases. As τ/τ_0 assumes very high values, the maximum driving force of 1.0 is approached; further decreases in σ_3 simply reduce the current through that path. In the one-compartment model, maximum inward current occurs when τ/τ_0 is ~2.

When the membrane conductance, σ_λ, approaches infinity, the system collapses into a first-order one in which the conductance is the parallel combination of the extracellular and cellular conductances, σ_1 and σ_c, and the capacitance is the sum of Γ_1 and Γ_2. That is, there is simply nontortuous diffusion into a single uniform compartment. When σ_λ approaches zero, E comes to equilibrium before there has been any uptake by C. The system becomes uncoupled; E follows the kinetics of M and C obeys a first-order equation in which the forcing function is 1.

Effect of increasing compartment number: When k is chosen to be 2, 3, or 4, the general relations obtained are similar to those depicted in Fig. 5. R still falls monotonically and passes through its equilibrium value when τ/τ_0 is 1. The curve is somewhat less steep than for the one-compartment case, but the differences are not very great. The relation between $\dot{R}$ and τ/τ_0 is shifted a bit to the left and shows a broader maximum, but again, the differences are minor. The increased precision obtained from using several compartments does not seem to warrant the increase in computational difficulty.

Comparison with the Crank model: Differences between these models are important only when τ/τ_0 is low. At high values of τ/τ_0, the models behave in a similar fashion. In a Crank model, the outermost portion of the tissue can take solute directly from the bathing solution, whereas the inner portions become exposed to the solute only after it has diffused through the extracellular space. The behavior of the outer compartment is similar in both models. However, the fact that the outer compartment fills rapidly has no effect on the other compartments of a Crank model. A succinct statement of the difference between the Crank model and the model developed here is that, in the Crank model, the results in the outermost layer do not affect the uptake in the rest of the tissue, whereas in the present model, all layers are coupled.

In the Crank model, material arrives at an interior extracellular point only by diffusion through the extracellular path. Even when σ_λ is very high, this diffusion limits the rate of entry of total material into the tissue. This tortuous diffusion process produces an upper limit to R.

The value of the upper limit is determined by the diffusion coefficient of the solute, the tortuosity, the thickness of the tissue, and time. For the mouse diaphragm at 30 s, this maximum value is 1.30. All of the normal data collected when lactate concentration was low showed higher values of R than 1.3. In the Crank model, $\dot{R}$ is always positive. Its value is greatest when σ_λ is infinite and it falls as the membrane permeability falls. Even though our data are not suitable for quantitative estimation of $\dot{R}$, it is clear that the derivative is not greatest when R is greatest. Indeed, the correlation is reversed. The results presented in Table II, both for R and its time derivative are incompatible with the Crank model. They do fit the model proposed here.

Approximation to the solution: Eq. 16 is cumbersome to work with and the physical behavior is not obvious. So long as R changes with time in a linear fashion, a useful simplification can be made. This approximation is within 5% of the real solution as long as the time is <0.2 of the shorter time constant. When this condition is met, R can be described by Eq. 19.

$$R = [1 + (\sigma_2/\sigma_1)] + (\sigma_2/2\,\Gamma_1)\,[1 - (\tau_0/\tau)]t. \tag{19}$$

Eq. 17 is the constant term of this relation, an expression of the fact that R was changing slowly in the present experiments. The coefficient of t in Eq. 19 shows the way $\dot{R}$ behaves. Although Eq. 16 was used for Figs. 4 and 5, Eq. 19 produces indistinguishable results except for the nonlinear portion of Fig. 5 *a*. This nonlinearity occurred at low values of τ/τ_0 and at those values, 30 s was no longer very small with respect to the shorter time constant, τ. At an earlier time, Fig. 5 *a* would be linear to lower values of τ/τ_0.

Quantitative Application of the Model to Mouse Data

The model was developed using fixed conductances. Eq. 18 can be used to choose a single value of the membrane conductance to match the experimental data. When carrier-mediated transport is present, however, σ_λ is not constant, but is a function of the lactate concentration on both sides of the cell membrane. The value of σ_λ obtained from Eq. 18 is really a one-compartment equivalent conductance. It is an average of the different values found at different depths in the tissue. σ_λ is a chord conductance, that is, it is the ratio of the flux to the driving force. If transport is only by free diffusion, this conductance is independent of the driving force. When a carrier process is present, however, this chord conductance falls at high concentrations of solute, since the carrier-mediated flux saturates.

NORMALIZATION PROCEDURES Replication of the same experiment produced slightly different results. The variation might come from differences in fluid compartment volumes, cellular permeability, or from tortuosity, in addition to measurement error. A preliminary experiment was performed in which the variation in mannitol uptake between different pieces of the same tissue was compared to the variation between different mice. The variation between mice was much greater than that within each individual animal. Since R is a measure of τ/τ_0, it is necessary to find a normalization procedure for the difference in extracellular kinetics in order to estimate membrane permeability accurately. This normalization procedure can use the mannitol uptake data obtained from each experimental animal. Eq. 2 shows that the slope of the relation between M and time provides an estimate of the ratio of V_e to ϵ. Since only ϵ enters into Eq. 18, a second relation between V_e and ϵ is needed. This

relation might be derived from the assumption that these parameters are independent or it might be derived from any of several assumptions of relationship. Three possible normalization procedures were tested. The test consisted in applying each putative normalization procedure to all of the normal experiments and then comparing the total within-group variation. The assumptions were as follows:

(*a*) V_e and ϵ were really constant and that the variation observed in the mannitol uptake was random error. Therefore, use a fixed value of ϵ for all animals. This assumption implies that the data should be averaged directly.

(*b*) All the variation in mannitol kinetics came from variation in ϵ. V_e was the same for all animals. Therefore, use the free diffusion coefficient and the mannitol kinetics to compute ϵ for each animal from Eq. 2.

(*c*) Variation in the mannitol kinetics came from variation in both ϵ and V_e. Further, these variables are related because, as tissue swelling takes place, V_e rises and ϵ falls. Therefore, make an approximation to this inverse relation by assuming that the product of V_e and ϵ is constant. Use the mannitol kinetics and the average value of this product to compute ϵ from Eq. 2.

The second assumption led to a 40% increase over the direct averaging of the within-group variation. Evidently, this assumption does not describe the physical situation. The third assumption led to a reduction of the within group variation by about one third. In these incubated tissues, tortuosity decreased concomitantly with elevation of extracellular space. The conclusion is consistent with the progressive reduction of ϵ reported by Brookes and MacKay (1971). Because of the compensating nature of these two changes, the values of σ_λ computed from simple averaging were very near to those computed after the normalization procedure. Thus, although normalization does reduce the variation in the data and does suggest some of the physical processes occurring in an isolated tissue, it does not change the estimation of cellular permeability.

CALCULATION OF σ_λ There were three experimental values for each mouse, one for each time period. Calculation of σ_λ for each animal included the following three steps:

(*a*) Reject the data from any period for which the mannitol space was unreasonably high. The justification for this rejection and the criterion used have been given above.

(*b*) Determine the best relation between the mannitol space and root time. The regression is forced through zero. Use the slope of this regression to estimate Ve/ϵ according to Eq. 2 and the statement that the product of these variables is 1.385 ml/g (the average value for the whole set of data).

(*c*) Use the 30-s value of R to compute σ_λ according to Eq. 18.

Fig. 6 shows the average values of σ_λ obtained from both the normal and the inhibited preparations. Conductances for the two highest values of lactate were averaged and a single point was produced for which the average lactate concentration was 24.6 mM. In the normal preparation, conductance fell continuously as lactate concentration increased. This is the result expected from a system with a saturable carrier. The inhibitor CHC reduced conductance only slightly when external lactate was 2.83 mM. At higher concentrations of lactate, σ_λ was greatly reduced, but it showed no dependence on lactate concentration.

If we make the analogy between lactate transport and an enzyme reaction, the transport rate can be thought of as a velocity and the lactate concentration as a substrate concentration.

In these terms, Fig. 6 is a plot of v/S as a function of S. This plot is not commonly used, but it does have several advantages here. It is a direct reflection of the experimental measurements. Calculation of reaction velocity, for example, involves multiplying these conductances by the substrate concentration. Any error present in the conductance will be multiplied by the external concentration. Further, this plot is analogous to that used by Eggleton et al. (1928) and the forms of the relations can be readily compared. On this plot, a system that follows Michaelis-Menten kinetics will show a hyperbolic relation that falls with increasing substrate concentration. The horizontal asymptote will be zero. It is quite clear that our chord conductances do not approach zero in either the normal or the inhibited preparation. Rather, they approach a fixed positive value. Studies on this inhibitor have indicated that the concentration for 50% inhibition is <1 mM (Halstrap, 1976; Spencer and Lehninger, 1976). Since we used a concentration of 20 mM, it is reasonable to suppose that the carrier system was very strongly inhibited. It follows that the residual, concentration-independent conductance is a leak for free diffusion.

Since the two conductances are in parallel, we can estimate the carrier conductance simply by subtracting the leak conductance from the total uninhibited value. The product of the carrier conductance and the external lactate concentration gives the rate of carrier-mediated transport. Fig. 7 presents the computed transport velocities as a function of external lactate concentration. Lactate transport rises sharply with increasing external lactate concentration when lactate is low. Saturation occurs quite suddenly when lactate concentration is ~10 mM. This result is very similar to that found by Jorfeldt et al. (1978) on human leg muscle. The data can be fitted to Michaelis-Menten kinetics. The parameters for such a fit are: V_{max} = 35.2×10^{-4} μM/g tissue s and K_m = 7.55 mM. The fit of this relation to the data points is only fair. A much better description of the data is obtained if it is assumed that the carrier requires combination with two lactate molecules before transfer. The kinetics of such a system are like Michaelis-Menten kinetics except that lactate concentration appears as the square rather than the first power. K' is the square of the concentration at which half maximum velocity is attained. The solid line in Fig. 7 is the best fit of divalent enzyme kinetics to the mouse data.

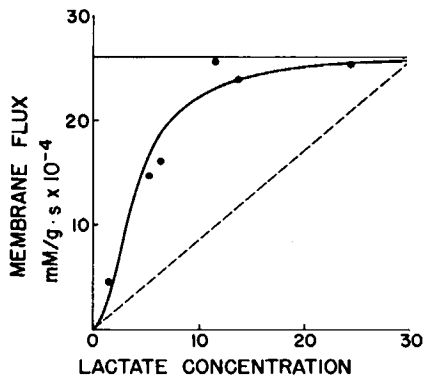

FIGURE 7 Transmembrane fluxes as a function of external lactate concentration. The points are the carrier-mediated fluxes. The heavy line is the divalent enzyme function with V_{max} = 26.2×10^{-4} μM/g · s and K' = 16.1 mmol/liter. The thin line is drawn at the maximum velocity. The dashed line represents the passive flux. The passive conductance is 0.86×10^{-4} ml/g · s.

With this fitting, V_{max} is 26.2×10^{-4} μM/g tissue s and K' is 16.1 mM. Hence, half maximum velocity is obtained when lactate concentration is 4 mM. The dashed line in Fig. 7 corresponds to the passive flux, using 0.86×10^{-4} ml/g tissue s for the free diffusion. The total flux is the sum of these two fluxes. When external lactate concentration is <10 mM, about three fourths of the total flux is carrier mediated. At higher concentrations, the passive flux accounts for a greater and greater fraction of the total and, when the external lactate concentration is 30 mM, the carrier and passive fluxes are equal.

COMPARISON WITH PREVIOUS EXPERIMENTS This same experiment has been done twice before. Eggleton et al. (1928) showed that the overall diffusion coefficient of lactate through frog muscle fell at high lactate concentrations. The range of concentration they used was from 8.6–40 mM. Their estimated diffusion coefficient was derived from the lactate space and their data are roughly equivalent to the data we presented in Table II. Their calculated diffusion coefficients fell to very low values when external lactate was high. It seems that the passive leak is less important in frog gastrocnemious than in mouse diaphragm. A plot of our carrier conductance as a function of substrate concentration could be formed by subtracting the passive conductance from the total conductances shown in Fig. 6. This carrier conductance relation would superpose on an Eggleton data. The carrier process has a similar value of K' in the two species.

Roos (1975) performed this experiment while addressing a different question. He was interested in the steady-state distribution of lactate and he therefore needed to know the duration of incubation required before steady state was attained. He expressed approach to steady state in terms of the ratio of intracellular to extracellular activities. This measure has the same meaning as does our measure of R. When lactate concentration was below 10 mM, steady-state values were obtained within 10 min. At higher concentrations, as much as 3 h was required to reach steady state. In the rat diaphragm preparation which he used, the time constant for diffusional entry is ~1 h (Creese, 1954; Brookes and MacKay, 1971). Thus, Roos was observing the steady-state distribution ratio quite early in the uptake process when lactate concentrations were low. His findings imply that $\dot{R}$ was always near zero at low concentrations of lactate, but that it was positive at early times when lactate concentration was high. They correspond to our findings on $\dot{R}$. The concentration dependence Roos found was similar to ours. The steady-state distribution ratio Roos found between cells and their surrounding fluid was 0.349 when the D-isomer of lactate was used. In a smaller number of experiments with the L-isomer, he found a value of 0.395. When $\dot{R}$ is zero, our data allow an estimate of this distribution ratio. The average value obtained when external lactate was <12 mM was 0.377.

Applicability of the Transient Analysis

A common experiment in the study of membrane transport properties is the immersion of an isolated tissue into a bath containing the material under investigation. Measurement of the steady-state ratio of cellular to extracellular concentrations can then lead to inferences about the presence of active transport. However, the steady-state method fails to distinguish between passive transport which occurs solely through physical diffusion and that which uses a carrier, i.e., facilitated diffusion. In sheets of epithelium, this distinction can be made by use of the Ussing criterion which relates the expected flux ratio across a membrane to the

electrochemical potential difference across that membrane (Ussing, 1949). However, this Ussing relation requires that concentrations be constant on both sides of the membrane for the period needed to make a flux measurement. In a tissue comprised of nonpolarized cells, the time required for an accurate flux measurement may be long with respect to the time-course of change of cellular composition. When this is the case and when co- or counter transport is not involved, no currently available method distinguishes between physical transport and facilitated diffusion. This report develops such a method.

Conclusions

We conclude that lactate crosses the muscle cell membrane by two mechanisms, free diffusion and a carrier system. At normal concentrations of lactate, the carrier system accounts for about three fourths of the transport. This system saturates quite sharply at ~10 mM and may require that two lactate molecules be combined with the carrier for transport. The rapid uptake of lactate observed requires that lactate be able to move both into and out of cells quickly. Hence, the carrier is bidirectional and acts as a facilitated diffusion rather than an active transport process.

This work was performed in partial fulfillment of the requirements of a Master of Science degree in Zoology at Washington State University.

Received for publication 16 December 1980 and in revised form 17 August 1981.

REFERENCES

Bendall, J. R., and A. A. Taylor. 1970. The Meyerhoff quotient and the synthesis of glycogen from lactate in frog and rabbit muscle. *Biochem. J.* 118:887–893.

Bretag, A. H. 1969. Synthetic interstitial fluid for isolated mammalian tissue. *Life Sci. Part I. Physiol. Pharmacol.* 8:319–329.

Brookes, N. and D. MacKay. 1971. Diffusion of labelled substances through isolated rat diaphragm. *Br. J. Pharmacol.* 41:367–378.

Crank, J. 1964. The Mathematics of Diffusion. The Oxford University Press, London, England. Chap. 8.

Creese, R. 1954. Measurements of cation fluxes in rat diaphragm. *Proc. R. Soc. Lond. B. Biol. Sci.* 142:497–513.

Eggleton, G. P., P. Eggleston, and A. V. Hill. 1928. The coefficient of diffusion of lactic acid through muscle. *Proc. R. Soc. Lond. B. Biol. Sci.* 103:620–628.

Evans, R. H., and J. W. Smith. 1976. The effect of catecholamines on the influx of calcium and the development of tension in denervated mouse diaphragm muscle. *Br. J. Pharmacol.* 58:109–116.

Glaviano, V. V. 1965. Distribution and gradient of lactate between blood and heart muscle. *Proc. Soc. Exp. Biol. Med.* 118:1155–1158.

Halstrap, A. P. 1976. Transport of pyruvate and lactate into human erythrocytes. *Biochem. J.* 156 (part 2):193–207.

Handbook of Chemistry and Physics. 1968. R. C. Weast, editor. Chemical Rubber Co., Cleveland. 48th edition.

Hirche, H., V. Hombach, H. D. Langohr, U. Wacker, and J. Busse. 1975. Lactic acid permeation rate in working gastrocnemii of dogs during metabolic alkalosis and acidosis. *Pfluegers Arch. Eur. J. Physiol.* 356:209–222.

Hirche, H., V. Hombach, H. D. Langohr, and U. Wacker. 1972. Lactic acid permeation rate in working skeletal muscle during alkalosis and acidosis. *Pfluegers Arch. Eur. J. Physiol.* 322(Suppl.):R75.

Jorfeldt, L., A. Juhlin-Dannfelt, and J. Karlsson. 1978. *J. Appl. Physiol.* 49:350–352.

Karlsson, J. 1971. Lactate and phosphagen concentrations in working muscle of man. *Acta. Physiol. Scand.* (Suppl.):358.

Karpatkin, S., E. Helmreich, and C. F. Cori. 1964. Regulation of glycolysis in muscle: effect of stimulation and epinephrine in isolated frog sartorius muscle. *J. Biol. Chem.* 239 (part 10):3139–3145.

Kubler, W., H. J. Bretschneider, W. Voss, H. Gehl, F. Wenthe, and J. L. Colas. Über die Milchsäure und Brenz traibensäurenpermeation aus dem hypothermen Myokard. *Pfluegers Arch. Eur. J. Physiol.* 287:203–233.

Lowry, O. H. 1972. A Flexible System of Enzymatic Analysis. Academic Press, Inc., New York. 194–196.

Mainwood, G. W., and P. Worsley-Brown. 1975. The effects of extracellular pH and buffer concentration on the efflux of lactate from frog sartorius muscle. *J. Physiol. (Lond.)* 250:1–25.

Milne, M. P., B. H. Scribnes, and M. A. Crawford. 1958. Nonionic diffusion and the excretion of weak acids and bases. *Am. J. Med.* 24:709–729.

Orloff, J., and R. W. Berliner. 1956. The mechanism of excretion of ammonia in the dog. *J. Clin. Invest.* 35:223–235.

Roos, A. 1975. Intracellular pH and distribution of weak acids across cell membranes. A study of D- and L-lactate and of DMD in rat diaphragm. *J. Physiol. (Lond.)*. 249:1–25.

Spencer, J. L., and A. Lehninger. 1976. L-lactate transport in Ehrlich ascites tumor cells. *Biochem. J.* 154 (part 2):405–414.

Ussing, H. 1949. The distinction by means of tracers between active transport and diffusion. *Acta Physiol. Scand.* 19:43–56.